

Article

# Predicting the Carbon Price Sequence in the Shenzhen Emissions Exchange Using a Multiscale Ensemble Forecasting Model Based on Ensemble Empirical Mode Decomposition

Jianguo Zhou <sup>1</sup>, Xuechao Yu <sup>1,\*</sup> and Xiaolei Yuan <sup>2</sup>

<sup>1</sup> Department of Economics and Management, North China Electric Power University, 689 Huadian Road, Baoding 071000, China; dldxzjg@126.com

<sup>2</sup> State Grid of Dezhou Power Supply Company, 1237 New Lake Street, Dezhou 253000, China; ylgw0534@126.com

\* Correspondence: yuxuechao121@163.com; Tel.: +86-159-3223-5607

Received: 23 June 2018; Accepted: 13 July 2018; Published: 21 July 2018



**Abstract:** Accurately predicting the carbon price sequence is important and necessary for promoting the development of China's national carbon trading market. In this paper, a multiscale ensemble forecasting model that is based on ensemble empirical mode decomposition (EEMD-ADD) is proposed to predict the carbon price sequence. First, the ensemble empirical mode decomposition (EEMD) is applied to decompose a carbon price sequence, SZA2013, into several intrinsic mode functions (IMFs) and one residual. Second, the IMFs and the residual are restructured via a fine-to-coarse reconstruction algorithm to generate three stationary and regular frequency components that high frequency component, low frequency component, and trend component. The fluctuation of each component can effectively reveal the factors that influence market operation. Third, extreme learning machine (ELM) is applied to forecast the trend component, support vector machine (SVM) is applied to forecast the low frequency component and the high frequency component is predicted via PSO-ELM, which means extreme learning machine whose input weights and bias threshold were optimized by particle swarm optimization. Then, the predicted values are combined to form a final predicted value. Finally, using the relevant error-type and trend-type performance indexes, the proposed multiscale ensemble forecasting model is shown to be more robust and accurate than the single format models. Three additional emission allowances from the Shenzhen Emissions Exchange are used to validate the model. The empirical results indicate that the established model is effective, efficient, and practical in terms of its statistical measures and prediction performance.

**Keywords:** carbon price sequence; Shenzhen emission exchange; ensemble empirical mode decomposition; multiscale ensemble forecasting model

## 1. Introduction

Global warming caused by greenhouse gas (GHG) emissions poses a severe challenge to the survival and development of human societies. China has been facing an unprecedented international pressure to curb its carbon emissions since it surpassed the United States (US) and became the largest carbon emitter in 2007 [1,2]. In response to the challenge of climate change, the Chinese government has promised that carbon intensity will be reduced by 40–45% in 2020 as compared with the 2005 level [3] and it has made a commitment to reduce carbon intensity by 60–65% in 2030 when compared with the 2005 level. The planned peak reduction in carbon emissions will occur in approximately 2030. When considering that China is undergoing rapid industrialization and urbanization, the Chinese

government has realized that it may not be easy to achieve the commitment of carbon emission reduction through traditional measures and proposals. Thus, the government must introduce a market-based emission reduction measure: the carbon emission trading scheme (ETS). In other words, the goal of carbon emission reductions allocated through market means allows for participants to achieve their own interests and needs. This approach has been deemed the most efficient emission reduction method [4]. Meanwhile, the operation mechanism of the energy market also has an impact on the ETS. Fossil energy consumption through power generation enterprises is the main source of carbon emissions [5]. There is an inherent transmission mechanism among the energy market, the electricity market and the carbon trading market. Different fossil fuel prices in the energy market have different effects on the carbon price in the carbon market. For example, the impact of oil price changes on carbon prices has been greater than coal prices and natural gas prices in EU ETS. However, oil prices are rising due to the gradual increase of oil consumption. For cost reasons, people tend to increase the use of cheaper coal, resulting in an increase of carbon dioxide emissions. This requires more carbon emissions quotas in order to promote the rise of carbon prices. When oil prices fall, people generally use less coal and reduce carbon dioxide emissions, resulting in decline in carbon prices. Although energy prices and electricity prices have affected the ETS, the carbon price is the most direct and effective reflection of the ETS. The volatility and predictability of the carbon price has become a popular topic. Thus, it is necessary and significant to improve the prediction accuracy of the carbon price. Accurate predictions can reflect the volatility of the carbon price and encompass the general trends in the carbon market to establish stable and effective market mechanisms. Additionally, predictions can provide effective guidance for investment decisions and help to avoid the maximization of carbon price risks.

Currently, most researchers focus on forecasting carbon price in the European market because it is the world's largest carbon trading market with the longest implementation history. In fact, since its initiation in 2005 [6], the institutions and rules of the European Union Emissions Trading Scheme (EU ETS) have been constantly improved to address issues with the market mechanism and market operation to enhance market efficiency and integrity. For this reason, carbon prices and the relevant energy prices that are associated with the carbon trading market have attracted widespread attention. The analysis and prediction models of these prices can generally be divided into two categories: econometric models and artificial intelligence models. The former mainly contains linear regression analyses [7], such as ARIMA [8], GARCH-type [9–11], and ARIMA-GARCH [12]. The latter contains ANN-type [13,14] and support vector machine (SVM)-type models [15,16]. The abovementioned methods are not robust for accurately forecasting carbon prices because of the nonstationary and nonlinear characteristics of these prices. Empirical mode decomposition (EMD) was proposed by Huang and his co-authors in 1998 and it has been widely applied to signal denoising [17,18]. This method has gradually spread for use in handling nonlinear and nonstationary time sequences. EMD is essentially different from the Fourier transform and wavelet decomposition methods, as it disassembles the original signal into several intrinsic mode functions (IMFs) plus a residual. These components of the input are used for econometric models and artificial intelligence models. For example, EMD-GAANN [19] was proposed to evaluate the two main future carbon prices from the ECX market. The proposed EMD-LSSVM [20] is more robust for carbon price forecasting in terms of its statistical measures and trading performance. Although the accuracies and fitting degrees of these forecasting models can be enhanced, the EMD has an obvious drawback—the frequent appearance of mode mixing. The core of ensemble empirical mode decomposition (EEMD), as proposed by Wu and Huang [21], is to add Gaussian white noise to overcome the stated drawback. For instance, EEMD-EELM [22], CEEMD-EELM [23], EEMD-DAN2-ALLN [24], and EEMD-APSO-RVM [25] were used to predict crude oil prices for the first time, and all achieved more precise predictions. Feng et al. utilized the variance ratio and EEMD to analyze the carbon price volatility factors in the EU ETS [26]. Zhu et al. proposed EEMD-HLT-LSSVM model for carbon price forecasting in the EU ETS [27]. Overall, few studies of the carbon prices using EEMD-type models have been published. There is a lack of domestic and international literature on the volatility analysis and predictability models of the carbon

prices of the seven pilot carbon trading markets in China. Because the carbon trading markets have a short run time and imperfect implemented trade mechanisms, data concerning the carbon trade are relatively limited. The carbon price sequence was decomposed into seven IMFs using the EEMD to study the market formation mechanism [28]. Li et al. forecasted five pilot market carbon prices using the EMD-GARCH model and then employed a CPB-CGE model to set a unified interval of the carbon price benchmark [29]. With the improvements in China's carbon market, increasing numbers of scholars be concerned with the analysis and prediction of carbon prices.

In summary, the analysis and prediction of carbon prices is still in its infancy in the carbon trading market. The following deficiencies exist: (1) the econometric models are applied to linear regression analyses in regular time series; the artificial intelligence models are not robust for accurately forecasting carbon prices that have the characteristics of the nonstationary and nonlinear. One bad problem is mode mixing in EMD algorithm, which methods can analyze the characteristics of carbon prices. However, the associated accuracy is limited. (2) There is little literature regarding the accurate forecasting of the carbon price in the Chinese market. However, some works have confirmed that the fluctuations of regional carbon prices in China are basically the same as those of the international carbon prices [30,31]. This article can draw on the methods used to study international carbon prices to analyze and predict carbon price fluctuations in the Chinese market. Therefore, this study seeks to address this gap with regards to how to improve the prediction accuracy of carbon price in the Chinese market.

In this article, a multiscale ensemble forecasting model is constructed based on EEMD, which is called EEMD-ADD. First, the carbon price is decomposed into several IMFs and one residual. Second, these IMFs and the residual are restructured into three stationary and regular frequency components. Finally, three different forecasting models are used to predict the components, and the predicted values are combined to form a final predicted value. The multiscale integrated prediction method overcomes the nonlinear and nonstationary issues that are associated with determining the carbon price and effectively improves the prediction precision.

The remainder of this paper is organized as follows: Section 2 shows a brief description of EMD, EEMD, SVM, and PSO-ELM and proposes the frame work of the EEMD-ADD model; Section 3 decomposes and analyses the carbon price sequence of SZA2013, and then introduces the necessary conditions for the proposed prediction model. Section 4 analyzes the simulation results; Section 5 provides three additional carbon price series forecasting cases; and, Section 6 concludes the paper based on the experimental results, briefly detailing future work.

## 2. Methodology

### 2.1. The Fundamentals of EEMD

EMD is an efficient and adaptive analysis method for handling nonlinear and nonstationary time series data. The principle of the EMD states that a signal is divided into data sequence of waveforms or trends at different scales via iterative steps. Each sequence serves as an IMF, which satisfies the following two criteria: (1) these functions have the same numbers of extremum and zero-crossings or differ at the most by one over the entire time series; and, (2) these functions have upper and lower envelopes with means of zero [17]. The IMFs and a residual component are given in Equation (1):

$$x(t) = \sum_{i=1}^n c_i(t) + r(t) \quad (1)$$

where  $x(t)$  is the original signal, each  $c_i(t)$  represents the  $i$ -th IMF, and  $r(t)$  is the residual component. The detailed EMD procedure is briefly expressed in Algorithm 1.

**Algorithm 1.** EMD Algorithm

---

Step 1: Mark the original signal as time series  $x(t)$ , Identify all the maxima and minima of  $x(t)$  and generate its upper and lower envelopes,  $a(t)$  and  $b(t)$ , via cubic spline interpolations.  
 Step 2: Compute the mean values  $m(t)$  of the envelopes ( $m(t) = [a(t) + b(t)]/2$ ).  
 Step 3: Calculate the difference ( $c(t) = x(t) - m(t)$ ).  
 Step 4: Check the properties of  $c(t)$ . If  $c(t)$  cannot satisfy the two criteria of the IMF, let  $x(t) = c(t)$ , and return to the step 1; otherwise,  $c(t)$  is defined as an IMF, and let the residual  $r(t) = x(t) - c(t)$ .  
 Step 5: Repeat steps 1–4 only when the termination criterion is satisfied.

---

However, the mode-mixing problem is an unavoidable drawback of EMD. Mode mixing is defined as an IMF containing several characteristic scales with considerable differences or having similar characteristic scales that are distributed over different IMFs, which causes the EMD to not present the characteristics of the original sequence. To overcome this issue, a Gaussian white noise is used in the original sequence analysis method known as the EEMD. Huang adds white noise into decomposed signal in order to supplement some frequency scales that are aimed at achieving better decomposition results. Because the general signals were decomposed via EMD missing frequency scales, the phenomenon of mode mixing appeared. EEMD could accurately decompose the original signal including fundamental component, harmonic component, and noise interference component into relative stationary modal components at various frequencies. Because it is based on an important ideology that the signal is composed of oscillations of different time scales, which is basically the same as the core ideas of Fourier Transformation. The procedure of the EEMD is briefly detailed in Algorithm 2.

**Algorithm 2.** EEMD Algorithm

---

Step 1: Add a group of Gaussian white noise into the original sequence.  
 Step 2: Decompose the integrated sequence into IMFs via the EMD algorithm.  
 Step 3: Repeat steps 1–2 with different scales of Gaussian white noise each time to obtain the corresponding IMFs.

---

Gaussian white noise has the characteristics of an irrelevant random sequence and a zero mean. In the process of making the ensemble mean, the signals are continuous at different scales and effectively avoid mode mixing, making the final decomposition of the IMFs able to maintain physical uniqueness, thus improving the signal denoising. A well-established statistical rule was proven to control the effect of the added Gaussian white noise, as given in Equation (2):

$$\varepsilon_n = \frac{\varepsilon}{\sqrt{N}} \quad (2)$$

where  $N$  is the number of ensemble members,  $\varepsilon$  is the amplitude of the added Gaussian white noise, and  $\varepsilon_n$  is the final standard deviation of the error, which is defined as the difference between the targeted signal and the corresponding IMFs. In general, the number of ensemble members ( $N$ ) is often set to 100, and the selected optimal standard deviation ( $\varepsilon$ ) from 0.1 to 0.2 is established by the  $k$ -fold cross-validation method.

## 2.2. The Fundamentals of Artificial Intelligence

### 2.2.1. Support Vector Machine

The SVM, as proposed by Cortes and Vapnik [32], is a new sort of machine learning algorithm that was based on Vapnik-Chervonenk dimension theory and the structural risk minimization (SRM) of statistical learning theory. The SVM maps the input variables on a high-dimension space kernel function, which comprises nonlinear transformations [33]. The selections of the penalty parameter ( $c$ ), kernel function parameter ( $g$ ), and  $\varepsilon$ -loss function parameter ( $p$ ) are vital because the forecasting performance of the SVM is impacted by these key parameters. There is an emphasis on selecting the

best kernel function, which is shown to be the radial basis function (RBF), which is simple, reliable, and efficient [34]. The procedure of the SVM is briefly expressed in Algorithm 3.

---

**Algorithm 3.** SVM Algorithm

---

Step 1: Preset training set  $T = \{(x_1, y_1), \dots, (x_l, y_l)\} \in (X \times Y)^l$

where  $x_i \in X = R^n, y_i \in Y = \{1, -1\} (i = 1, 2, \dots, l)$ ;  $x_i$  is a feature vector.

Step 2: Select appropriate kernel function  $K$  and parameter  $C$ . Construct and solve the optimization problem.

$$\min_a \frac{1}{2} \sum_{i=1}^l \sum_{j=1}^l y_i y_j a_i a_j K(x_i, x_j) - \sum_{j=1}^l a_j$$

$$s.t. \sum_{i=1}^l y_i a_i = 0, 0 \leq a_i \leq C, i = 1, \dots, l$$

Derive the optimal solution  $a^* = (a_1^*, \dots, a_l^*)^T$ .

Step 3: Select a positive component  $0 < a_j^* < C$  of  $a^*$  and calculate the threshold

$$b^* = y_j - \sum_{i=1}^l y_i a_i^* K(x_i - x_j)$$

Step 4: Construct decision function

$$f(x) = \text{sgn}(\sum_{i=1}^l a_i^* y_i K(x, x_i) + b^*)$$


---

### 2.2.2. Particle Swarm Optimization and Extreme Learning Machine

The PSO, as proposed by Kennedy and Eberhart [35], is a stochastic optimization algorithm that simulates the social behavior of biological organisms, such as birds [36]. For particle optimization, each particle indicates a candidate solution of the problem within an  $n$ -dimensional search space, which is initialized via the process of iterations by position, velocity, and fitness value. The velocity represents the direction and distance of the particle flight [37].

Extreme learning machine (ELM) was proposed as a new type of single-hidden-layer feed forward neural network (SLFN) by Huang et al. [38]. The algorithm randomly generates the connection weights between the input layer and the hidden layer, and the output weights between the hidden layer and the output layer are acquired via the least squares method while using the minimizing squared loss function. In the training process, the parameters do not need to be adjusted, and the unique optimal solution can be acquired once the number of hidden layer neurons is set. The process of selecting the network parameters effectively avoids the number of iterations and significantly reduces the adjustment time of the network parameters. When compared with traditional training algorithms, the ELM has the advantages of fast learning and good generalization performances [39]. The procedure of PSO-ELM is briefly described in Algorithm 4.

---

**Algorithm 4.** PSO-ELM Algorithm

---

Step 1: Preset training set,  $N = \{(x_i, y_i)\} | x_i \in R^n, y_i \in R, i \in [1, m]$  with the activation function  $g(x)$ , and the number of hidden layer neurons  $N$

Step 2: Generate random values for the weights  $w_i$  and bias  $b_i, i \in [1, N]$

Step 3: Initialize the particle swarm, and randomly set the population, position and velocity of each particle.

Step 4: Calculate the fitness and update the velocity and the position parameters.

Step 5: Output the optimal  $w$  and  $b$  parameters.

Step 6: Calculate the hidden layer output matrix,  $H$ ,

$$H = \begin{bmatrix} g(w_1 x_1 + b_1) & \cdots & g(w_N x_1 + b_N) \\ g(w_1 x_2 + b_1) & \cdots & g(w_N x_2 + b_N) \\ \vdots & \cdots & \vdots \\ g(w_1 x_N + b_1) & \cdots & g(w_N x_N + b_N) \end{bmatrix}$$

Step 7: Calculate the output weight,  $\beta = H^\dagger Y$ , where  $H^\dagger$  is Moore-Penrose pseudoinverse [35], and the label matrix of the training set is  $Y = [y_1, y_2, \dots, y_N]^T$

Step 8: Obtain output weights,  $\beta$

---

### 2.3. The Fundamentals of the EEMD-ADD Model

A multiscale ensemble forecasting model based on the EEMD algorithm (EEMD-ADD) of the carbon price in China's regional carbon trading market are constructed, as shown in Figure 1. The model ordinarily comprises four key steps:

- Step 1: Each nonlinear nonstationary carbon price sequence is decomposed into several stable regular IMFs and one residual via EEMD.
- Step 2: The IMFs are separated into high-frequency components and low-frequency components by a fine-to-coarse reconstruction algorithm, and the residual is the trend component.
- Step 3: PSO-ELM is applied to predict the high-frequency component, SVM is applied to predict the low-frequency component, and ELM is applied to predict the trend.
- Step 4: The predicted values of the three components are assembled into the final forecast values and are compared with the original carbon price sequence.

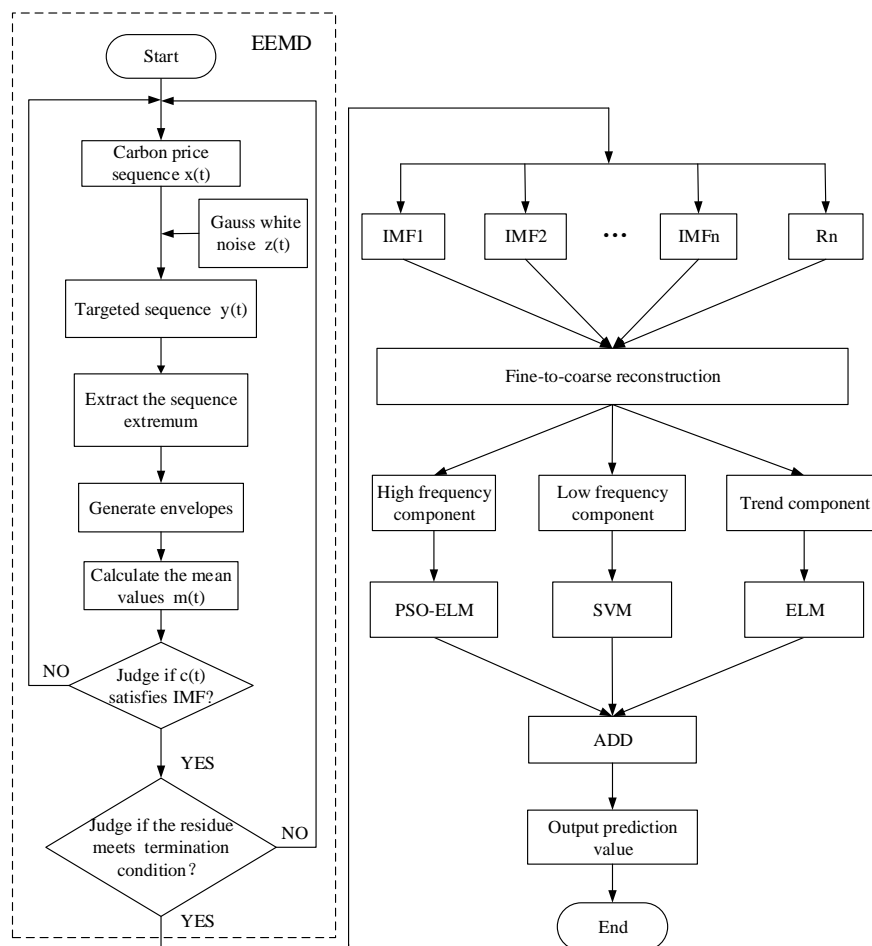


**Figure 1.** The framework of the proposed ensemble empirical mode decomposition (EEMD-ADD) model.

## 3. Empirical Analysis

### 3.1. Data Selection and Test

The Shenzhen Emissions Exchange is the first regional carbon trading market in China and has the most comprehensive operational structure. It accounts for 12.6% of the country's total trading volume, 22.85% of the total trading value, and only 2.5% of the total allowances. The allowance circulation

rate is ranked first and the market has been open to foreign investors in the pilot cities for many years, which has led to financial carbon innovations. In this paper, the Shenzhen Emissions Exchange is used to represent China’s carbon trading market. The carbon price sequence of SZA2013 from 1 November 2013 to 30 June 2017, excluding public holidays, with a total of 882 observations, was chosen as an experimental sample. The carbon price sequence is shown in Figure 2 and Table 1.

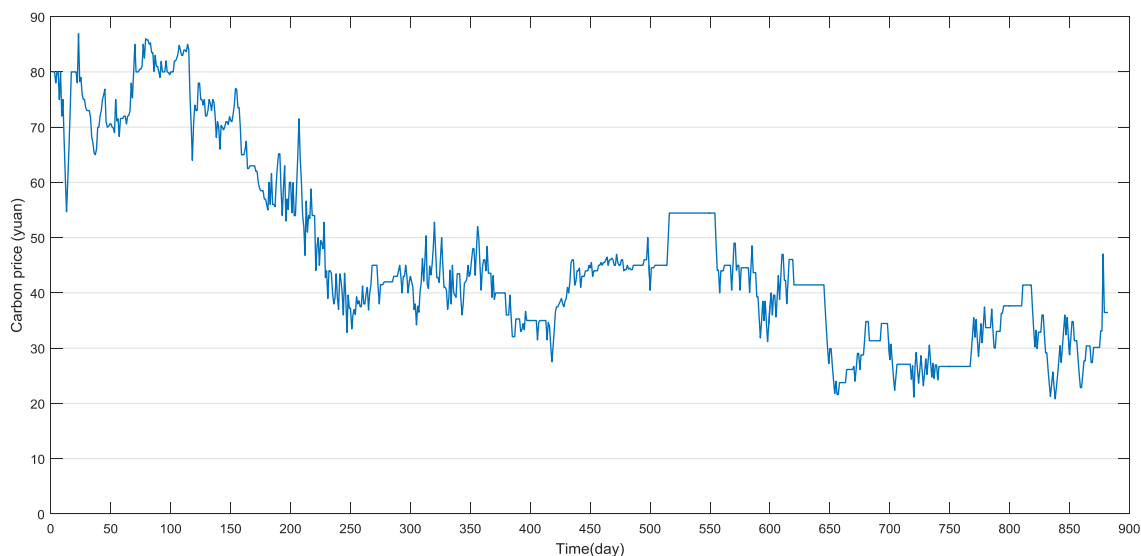


Figure 2. The carbon price fluctuations of SZA2013.

Table 1. Statistical descriptions of the carbon price of SZA2013.

Sample	Mean	Standard Deviation	Median	Maximum	Minimum	Skewness	Kurtosis
882	46.46	16.43	43.00	86.9	20.82	0.80	−0.32

The price fluctuation sequence of SZA2013 is obviously irregular. In its early stage, this series has a fast downward trend. In its later stage, the price is slightly stable and it has a slower downward trend. The overall trend does not meet the normal distribution. Accounting for the above statistical characteristics, the augmented Dickey-Fuller (ADF) method is used to test the price stationarity, and the Brock-Dechert-Scheinkman (BDS) method is used in order to test the linear characteristics of the price. Table 2 shows the stability test results of the carbon price sequence based on the ADF. This statistic meets the critical values of the 1% and 5% significance levels and it is less than the critical value of the 10% significance level. Moreover, the *p*-value is 0.0756. This sequence is clearly nonstationary. Table 3 shows the linear test result of the carbon price sequence based on the BDS. The embedding dimension gradually increased and the corresponding BDS statistical value also increases. The corresponding *z*-statistic is greater than the critical value. The relevant *p* value is zero, i.e., less than 0.05. Thus, this sequence is nonlinear.

Table 2. The stability test of carbon price sequence of SZA2013.

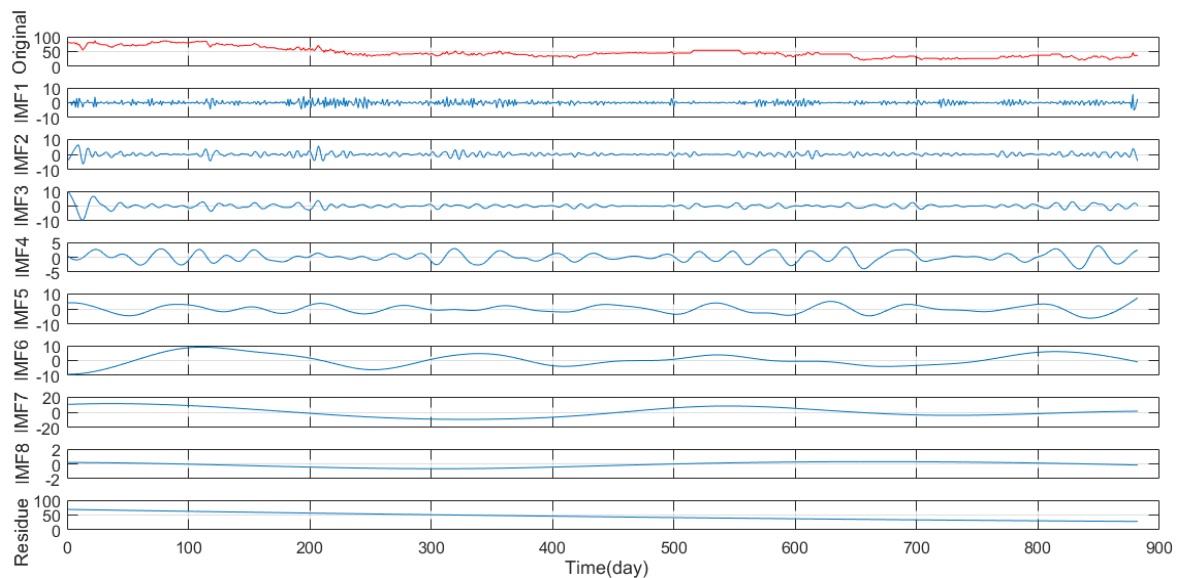
Variable	ADF Statistics	Critical Value (Significance Level)
Carbon price	−3.2496	−3.9685 (1% level)
		−3.4149 (5% level)
		−3.1296 (10% level)

**Table 3.** The linearity test of the carbon price sequence of SZA2013.

Dimension	BDS Statistic	Std. Error	z-Statistic	Prob.
2	0.1903	0.0026	72.4668	0.0000
3	0.3253	0.0042	78.1989	0.0000
4	0.4189	0.0049	84.8156	0.0000
5	0.4836	0.0051	94.2111	0.0000
6	0.5279	0.0049	106.9743	0.0000
7	0.5578	0.0045	123.7421	0.0000
8	0.5776	0.0040	145.4268	0.0000

### 3.2. Data Processing and Analysis

Given the above test, China's regional carbon trading product price sequence has nonstationary and nonlinear characteristics, making the sequence fluctuation characteristics basically the same as the price fluctuation characteristics in the international market of the EU ETS. The IMFs and the residual of the SZA2013 price sequence are derived by applying the EEMD, as shown in Figure 3.

**Figure 3.** The decomposition of the SZA2013 sequence using the EEMD.

#### 3.2.1. The Analysis of IMF Statistics

In this EEMD, an ensemble of 100 members is created, and the added Gaussian white has a standard deviation of 0.2. The carbon price sequence is divided into eight IMFs and one residual. Preliminary observation show that the frequencies range from high to low and the amplitudes become generally larger. The frequency variations of IMF1 and IMF2 are approximately the same as those of the local frequencies of the original sequence. The residual is the mode that slowly varies around the long-term average, with a trend that is nearly the same as that of the original sequence. To further study the eight IMFs and one residual, the mean period of each IMF, the correlation between each IMF and the original sequence, and the variance and variance percentage of each IMF are shown in Table 4. The mean period represents the ratio of each IMF's sample size to the number of its maximum points (or minimum points), which can be used to show the cycle length of the price-influencing factor or the reaction to fluctuations in the price sequence. IMF1-IMF3 has a mean period of less than 15 days, indicating that these are more intense fluctuations. IMF6-IMF8 is the other important mode, having a mean period of more than three months. The Pearson correlation coefficient is used to describe the linear correlation between the two sequences and the Kendall correlation coefficient is

used to determine whether the two sequences have a tendency to concurrently change. The residual has the highest correlation with the original sequence, up to 0.843 and 0.588, but almost no fluctuation. The correlation coefficients of IMF6-IMF8 are also relatively high, but that of IMF8 is negatively correlated with the original signal. The variances and percentages explained by each of IMF have fluctuating values. The higher the variance ratio, the greater the impact of the relevant IMF on the original sequence. The variance ratio of the residual is 55.23%, as this has the greatest influence on the original sequence. The trend of the residual is basically the same as that of the original sequence. Meanwhile, the sum of the variance ratios of IMF6-IMF8 is 18.65%. The trends of these three components show little similarity to that of the original sequence. It is important to emphasize that the total variances of the IMFs and residuals are not equal to the variances of the original sequence due to a combination of rounding errors, nonlinearities of the original sequence, and the introduction of variance by the treatment of the cubic spline end conditions.

**Table 4.** Measures of the intrinsic mode functions (IMFs) and the residual.

Sequence	Mean Period (day)	Pearson Correlation	Kendall Correlation	Variance	Variance as % of Original	Variance as % of ( $\Sigma$ IMFs + Residual)
Original	null	null	null	269.945	null	null
IMF1	2.96	0.091	0.062	1.716	0.64%	0.83%
IMF2	6.76	0.130 *	0.075	1.440	0.53%	0.70%
IMF3	13.16	0.147 *	0.094	2.161	0.80%	1.04%
IMF4	28.92	0.134 *	0.106 *	2.132	0.79%	1.03%
IMF5	70.56	0.22 *	0.171 *	6.250	0.23%	0.30%
IMF6	160.36	0.328 *	0.249 *	16.728	6.20%	8.03%
IMF7	441	0.657 *	0.386 *	32.948	12.21%	15.89%
IMF8	null	-0.279 *	-0.211 *	0.656	0.24%	0.32%
Residual	null	0.843 *	0.588 *	149.084	55.23%	71.86%
Sum	null	null	null	null	76.87%	100.00%

\*: Correlation is significant at the 0.01 level (2-tailed).

The IMFs are separated into high frequency and low frequency components based on a fine-to-coarse reconstruction algorithm [40], and the residual is the trend component. Each component has abundant economic meanings and it reveals some features of the carbon price. The mean of the algorithm departs significantly from zero at IMF 4 (Mean > 0.01), which is shown as a function of the IMF's K index in Figure 4. Therefore, the partial reconstruction using IMF1-IMF3 represents the high frequency components. The low frequency components comprise IMF4-IMF8 and the residual is considered to be the trend component.

Figure 5 shows the original price sequence and the three components, and Table 5 gives the statistical measures of these sequences, including the Pearson and Kendall correlations between each component and the original price, the variances of each component and the variance percentages. Each component has a specific meaning when combined with the carbon trading market situation.

**Table 5.** Correlations and variances of the components.

New Sequence	Pearson Correlation	Kendall Correlation	Variance	Variance as % of Original	Variance as % of ( $\Sigma$ IMFs + Residual)
Original	null	null	269.945	null	null
High frequency component	0.203 *	0.138 *	7.84	2.90%	3.46%
Low frequency component	0.653 *	0.420 *	69.223	25.64%	30.61%
Trend component	0.843 *	0.588 *	149.084	55.23%	65.93%
Sum	null	null	null	83.77%	100.00%

\*: Correlation is significant at the 0.01 level (2-tailed).

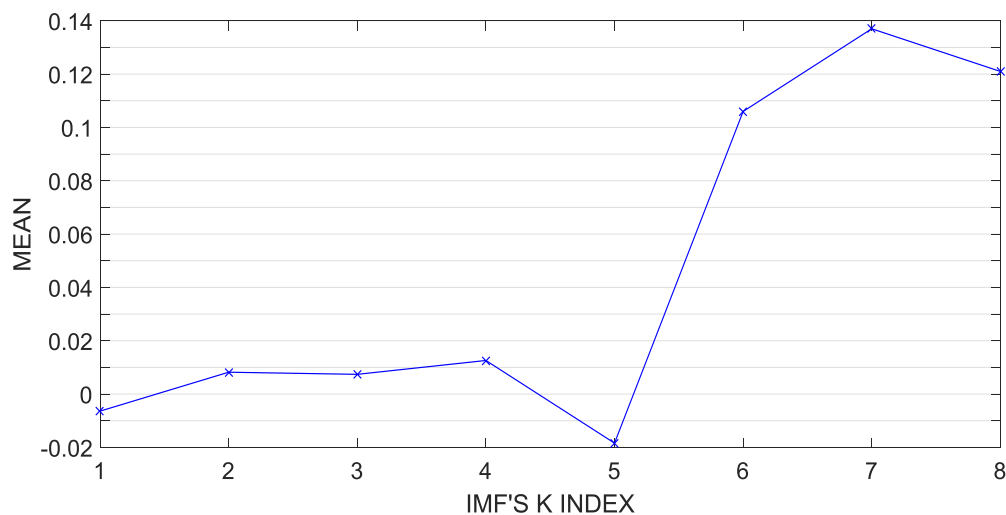


Figure 4. The mean of the IMF's K index.

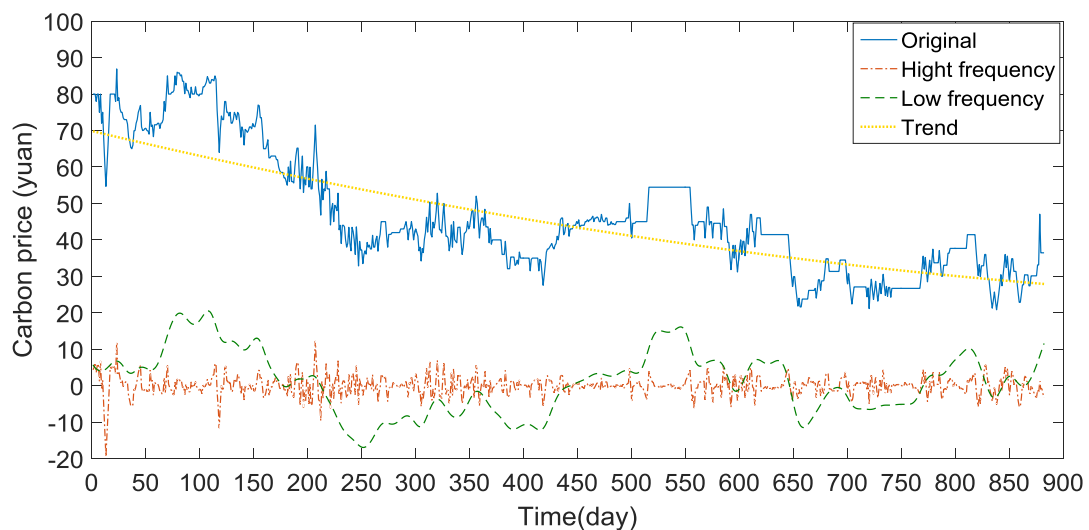


Figure 5. The three components of the original price sequence.

### 3.2.2. High Frequency Component—Short-Term Market Fluctuations

The high frequency component fluctuates about zero, which reflects the impact of the short-term market fluctuations that are caused by disequilibrium of supply and demand on the market mechanism. These fluctuations have a high occurrence frequency and a short continuous cycle with no serious impacts on the carbon price and can represent events such as the extreme weather conditions, e.g., strong typhoons, which have caused the Shenzhen ETS to close for short periods of time. The correlation coefficient and variance are relatively low when compared with those of the original price sequence. The high frequency fluctuation is shown to not be the main component of the price fluctuations and has little impact on the long-term carbon price trends. However, the high-frequency component fluctuations are becoming increasing frequent and will become the fundamental forces of carbon price fluctuations and carbon price changes. Thus, it is vital to establish the short-term carbon price rules.

### 3.2.3. Trend Component—Market Internal Mechanism

The trend component has a high correlation with the original price sequence and has a variance ratio that explains more than 50% of the variance of the carbon price sequence. Therefore, the trend

component reveals the long-term trend of the carbon prices and it is a deterministic factor in the long-term carbon price evolution, reflecting the impact of the internal market mechanisms on the carbon price. The mechanisms add carbon quota products per annum, expanding the market participants and transactions, and making the demand for a single quota product decline. Thus, the price has a steady downward trend. The value of the trend component is the highest, regardless of the Pearson correlation coefficient, Kendall correlation coefficient, or variance. The analysis results suggest that this component is the major component of the carbon price trend, determining the intrinsic value of carbon emissions and explaining fluctuation characteristics of the carbon price sequence. The value of this signal is to provide a reference for the long-term equilibrium price of the carbon market.

### 3.2.4. Low Frequency Component—Market Economy Periodicity and Significant Events

The low frequency component eliminates the short-term market fluctuations and long-term price trends, reflecting the impacts of market economy periodicity on carbon price. In addition, significant events, such as the global financial crisis, intergovernmental negotiations, and national allocation plans, are able to influence the carbon price trends. For example, the China Certified Emission Reduction (CCER) project was listed on the Shenzhen ETS in June 2015, causing a marked downward trend of the carbon price. Because the occurrences of significant events are not frequently, these impacts are reflected in the low frequency component. Significant events are indicated to affect the carbon price for a long period. However, the low frequency components have little ability to explain the overall market price fluctuations due to their low variance ratios.

With the gradual advancement of processes in China's carbon trading market, carbon prices will dominate the market. The fluctuations in carbon prices and the associated components can effectively reflect the overall operation of the market, including the instability and low efficiency of the carbon trading market. The internal market mechanism is imperfect and easily disturbed by external factors. Therefore, this paper studies the fluctuations in the carbon price and its component to determine the relative stability of China's carbon market and auxiliary multi-level carbon financial market system with the goal of the Chinese government to achieve carbon emission reductions.

## 3.3. Forecasting the Carbon Price Sequence

### 3.3.1. Model Performance Evaluation

To quantitatively examine the prediction performances of single format models, including PSO-ELM, SVM, ELM, and BPNN, as compared to that of EEMD-ADD, this paper applies the following error-type and trend-type performance measures. The root mean square error (*RMSE*), the mean absolute error (*MAE*), and the mean absolute percentage error (*MAPE*) are the error-type measurements utilized to evaluate the prediction errors. The Directional symmetry (*DS*), correct up-trend (*CP*), and correct down-trend (*CD*) are the trend-type performance measurements. *DS* indicates the accuracy of the predicted direction. *CP* and *CD* indicate the accuracies of the predicted upward and downward trends. These three indicators are used to evaluate the prediction accuracies. The algorithms for the six criteria are shown in Equations (3)–(8).

$$RMSE = \sqrt{\frac{1}{n} \sum_{t=1}^n |y_t - \hat{y}_t|^2} \quad (3)$$

$$MAE = \frac{1}{n} \sum_{t=1}^n |y_t - \hat{y}_t| \quad (4)$$

$$MAPE = \frac{1}{n} \sum_{t=1}^n \left| \frac{y_t - \hat{y}_t}{y_t} \right| \times 100\% \quad (5)$$

$$DS = \frac{100}{n} \sum_{t=1}^n a_t, a_t = \begin{cases} 1 & \text{if } (\hat{y}_t - \hat{y}_{t-1})(y_t - y_{t-1}) \geq 0 \\ 0 & \text{otherwise} \end{cases} \quad (6)$$

$$CP = \frac{100}{n_1} \sum_{t=1}^{n_1} a_t, a_t = \begin{cases} 1 & \text{if } (\hat{y}_t - \hat{y}_{t-1}) > 0 \text{ and } (\hat{y}_t - \hat{y}_{t-1})(y_t - y_{t-1}) \geq 0 \\ 0 & \text{otherwise} \end{cases} \quad (7)$$

$$CD = \frac{100}{n_2} \sum_{t=1}^{n_2} a_t, a_t = \begin{cases} 1 & \text{if } (\hat{y}_t - \hat{y}_{t-1}) < 0 \text{ and } (\hat{y}_t - \hat{y}_{t-1})(y_t - y_{t-1}) \geq 0 \\ 0 & \text{otherwise} \end{cases} \quad (8)$$

where  $y_t$  is the  $t$ -th actual value,  $\hat{y}_t$  is the  $t$ -th prediction value,  $n$  represents the number of evaluated data points,  $n_1$  is the number of data points ascending, and  $n_2$  is the number of data points descending. The smaller RMSE, MAE, and MAPE values indicate lower deviations of the prediction value from the actual values. The larger DS, CP, and CD values show higher accuracies of the prediction value.

### 3.3.2. Parameter Setting and Input Selection

In this paper, the three prediction models of PSO-ELM, ELM, and SVM are applied. In PSO, the initial population size is set to 40, the max-generation is 100, and the mutation probability is set to 0.6. Moreover, the range of the variance is  $[-5, 5]$  and the velocity range is  $[-1, 1]$ . In ELM, the number of hidden layer nodes is 10 in the trend component and 30 in the high frequency component due to their inherent characteristics. For the SVMs models, the  $\varepsilon$ -loss function parameter ( $p$ ) is set to 0.01. The penalty parameter ( $c$ ) and kernel function parameter ( $g$ ) are adjusted based on the validation sets. It is shown in Table 6. Per Section 3, the training dataset spans 1 November 2013, to 31 March 2017, providing a total of 799 observations, and the testing data spans 5 April 2017, to 31 June 2017, providing a total of 83 observations. It is shown in Table 7.

**Table 6.** The parameter setting of the algorithm.

Algorithm	Parameter	Value
PSO	Initial population size	40
	Max-generation	100
	Mutation probability	0.6
	Variance range	$[-5, 5]$
	Velocity range	$[-1, 1]$
ELM	Number of hidden layer nodes (trend component)	10
	Number of hidden layer nodes (high frequency component)	30
SVM	$\varepsilon$ -loss function parameter	0.01

**Table 7.** The data sets of SZA2013.

Label	Data	Number
Data sets	2013/11/1–2017/6/31	882
Training set	2013/11/1–2017/3/31	799
Testing set	2017/4/5–2017/6/31	83

## 4. Results

As Figure 6 shows, the relative errors of the three frequency components and the carbon price sequence are described via ELM, SVM, and PSO-ELM models. This analysis shows that (a) the range of relative errors of the trend component is from  $2.628 \times 10^{-6}$  to  $2.855 \times 10^{-6}$ , but the trend of the error gradually increases due to the effect of training set fitting. (b) The relative error of the low-frequency components is relatively stable, generally ranging between plus and minus 0.2. Nevertheless, four data points show errors that are greater than  $-0.4$  due to the corresponding points in the low frequencies

being biased against the trend of the overall low-frequency dataset. (c) It is difficult to obtain high accuracy predictions for the high-frequency component due to its violent fluctuations and nonlinear characteristics. However, the fluctuation range of the relative error is  $[-1, 1]$  due to its low amplitude. The predicted result of the PSO-ELM model shows a high accuracy. (d) The range of the errors of the carbon price sequence is generally between plus and minus 0.05. The range of fluctuations also shows a gradual decline. Therefore, the fitting effect and predicted result of the multiscale ensemble forecasting model are found to be great.

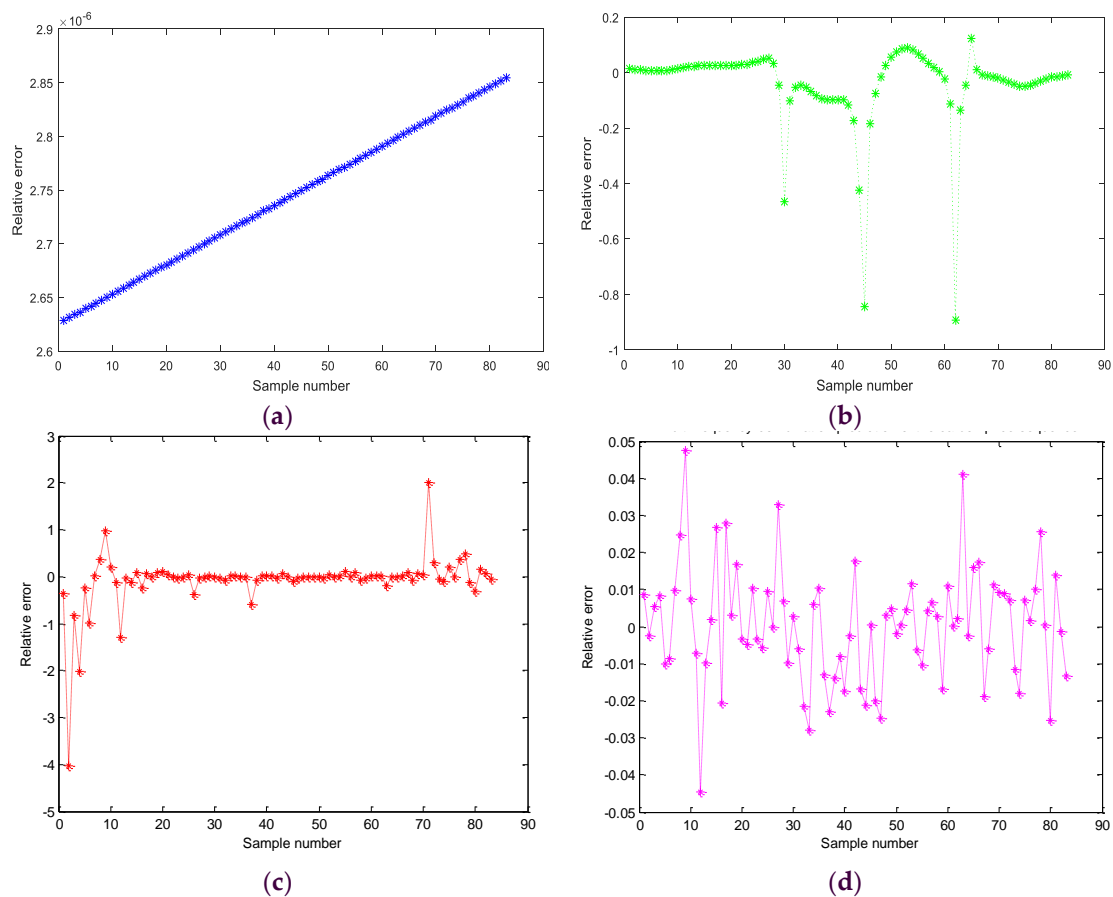


**Figure 6.** The relative errors of the three components and the carbon price sequence. (a) Extreme learning machine (ELM) prediction of the trend component; (b) Support vector machine (SVM) prediction of the low frequency component; (c) extreme learning machine whose input weights and bias threshold were optimized by particle swarm optimization (PSO-ELM) prediction of the high frequency component; (d) a multiscale ensemble forecasting model based on ensemble empirical mode decomposition (EEMD-ADD) prediction of the carbon price.

Figure 7 shows the forecasting results for the SZA2013 of Shenzhen ETS from the five forecasting models of EEMD-ADD, PSO-ELM, SVM, ELM, and BPNN. This analysis shows that (a) the goodness of fit of proposed EEMD-ADD model predicted values and the actual values is the highest, while that of the BPNN predicted values is the lowest. (b) The predicted precision of the multiscale ensemble forecasting model is superior to those of the corresponding single format models. Next, the statistical analyses of the five prediction models are given in Table 8. The results allow for the following conclusions: (a) the RMSE, MAE, and MAPE values of the error-type performance index analysis of the EEMD-ADD model are 0.5322, 0.3897, and 1.19, respectively. These values are smaller than those of the other single format models, which indicates that the multiscale ensemble forecasting model has the highest prediction accuracy. (b) The EEMD-ADD model has the largest DS, CP, and CD values

of the trend-type performance indexes, which are 95.18, 92.68, and 97.56, respectively. These results show that this method has a high accuracy when predicting the directions of the carbon price trend indexes. (c) The predictive performance of PSO-ELM is better than that of ELM due to the strong performance of the swarm intelligence algorithm. (d) The BPNN shows the worst performance among the five models due to its inherent characteristics that may lead to low efficiencies and local optimums. Moreover, the selection of the BPNN hidden nodes depends on trial and error procedures, thus making it difficult to obtain an optimal network that improves prediction performance. Thus, the EEMD-ADD has lower prediction errors and higher direction prediction accuracies of the carbon price than the PSO-ELM, SVM, ELM, and BPNN models.

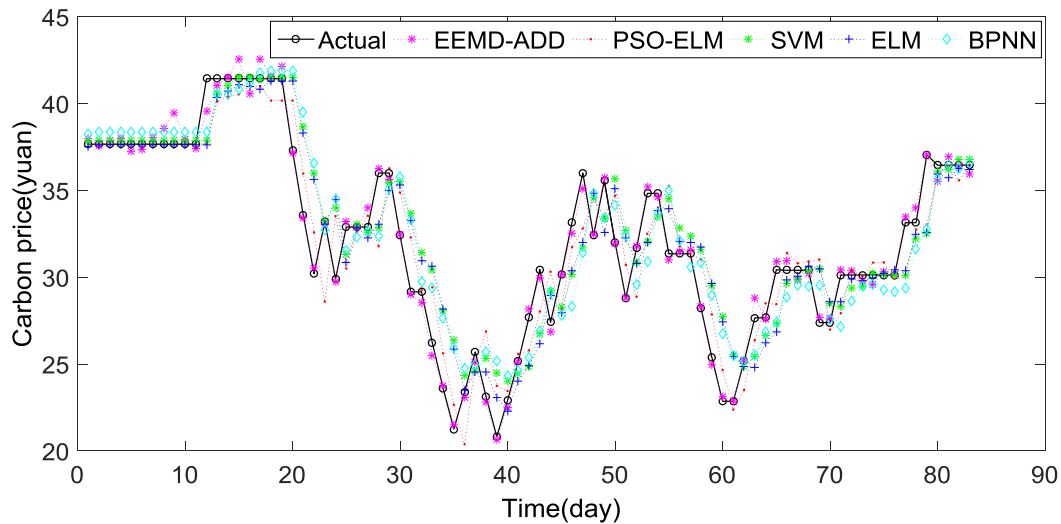


Figure 7. The results of the carbon price sequence predictions of the five models.

Table 8. The statistical values of the carbon price predictions of the five models.

Model	RMSE	MAE	MAPE	DS	CP	CD
EEMD-ADD	0.5322	0.3897	1.19	95.18	92.68	97.56
PSO-ELM	1.9654	1.4823	4.89	81.72	75.59	80.54
ELM	2.3089	1.7698	5.95	77.11	69.44	76.47
SVM	2.4075	1.7585	6.01	79.52	74.40	78.42
BPNN	2.4699	1.9088	6.38	74.7	70.07	72.11

### 5. Additional Forecasting Cases

For future investigations of the performance of the EEMD-ADD model, three additional carbon emission allowance products that are derived from Shenzhen ETS are applied in the paper. The relevant results are shown in Table 9.

Table 9. Data sets for three additional carbon emission allowance products.

Product	Data sets	Total Number	Training Set Size	Testing Set Size
SZA2014	2014/9/9–2017/6/30	683	600	83
SZA2015	2015/7/13–2017/6/30	485	435	50
SZA2016	2016/8/29–2017/6/30	226	190	36

As shown in Table 10, the analyses and their conclusions are similar to those made in Section 4. For each of the carbon quota products, the EEMD-ADD model has the best performance with lower prediction errors and higher direction prediction accuracies of the carbon prices than those of the

single format models of PSO-ELM, SVM, ELM, and BPNN. Horizontal comparisons of the carbon quota products show obvious differences in the sample size and price fluctuations. The single format models are mainly affected by the sample size. Large sample sizes can improve prediction accuracies. However, the EEMD-ADD model is not only affected by the sample size, but is also affected by the frequencies of the price fluctuations. Thus, the results demonstrate that the proposed model is more effective than the single format models for forecasting the carbon price sequence.

**Table 10.** The statistics of the three additional carbon emission allowance products.

Product	Model	RMSE	MAE	MAPE	DS	CP	CD
SZA2014	EEMD-ADD	0.3334	0.1063	0.53	97.59	94.41	90.67
	PSO-ELM	1.3538	0.9327	2.71	89.17	86.88	81.76
	ELM	1.7684	1.0604	3.17	86.75	83.87	80.04
	SVM	1.7674	1.0852	3.23	85.54	80.56	78.64
	BPNN	2.1464	1.4302	4.36	80.34	78.13	75.10
SZA2015	EEMD-ADD	0.197	0.0596	0.18	96.00	95.83	92.31
	PSO-ELM	1.6715	1.3427	3.88	80.00	78.26	76.00
	ELM	2.3311	1.9121	5.63	68.00	68.27	63.94
	SVM	2.3582	1.8338	5.47	68.00	68.00	63.64
	BPNN	2.6894	2.0991	6.06	66.00	62.18	59.36
SZA2016	EEMD-ADD	1.1404	1.2582	4.01	88.89	89.47	88.23
	PSO-ELM	2.1577	1.8232	5.99	63.88	64.71	63.05
	ELM	2.5891	2.2303	7.07	57.53	62.16	52.94
	SVM	2.781	2.4128	7.59	55.56	57.23	51.86
	BPNN	2.8977	2.8861	7.94	52.77	55.00	50.00

## 6. Conclusions and Future Work

This paper mainly proposes a multiscale ensemble forecasting model that is based on EEMD (EEMD-ADD) for carbon price sequences. Due to the volatility of carbon prices, EEMD is applied to decompose the fluctuations process into several IMFs and one residual. A fine-to-coarse reconstruction algorithm is employed to restructure the IMFs in order to generate three components that high frequency component, low frequency component, and trend component. The fluctuation of each component can effectively reveal the factors that influence market operation. The predicted values of the three frequency components via PSO-ELM, SVM, and ELM models are combined to derive the final forecasted values. Using the carbon price of SZA2013 in Shenzhen ETS for samples, the EEMD-ADD model has been empirically tested, demonstrating that its prediction performance is superior to that of single format models. The SZA2014, SZA2015, and SZA2016 can also prove the empirical result. Future work is proposed, as follows: (1) we should establish other decomposition algorithms and prediction models to further improve prediction performances. (2) We should obtain data from the other six pilot markets for longitudinal predictions and concurrent comparisons. (3) According to national policies and market evolution, scenario analyses should be studied to investigate the proposed model and achieve a maximum profit from the production and investment in China's carbon trading market.

**Author Contributions:** J.Z. conceived the overall structure of the paper. X.Y. (Xuechao Yu) wrote the paper. X.Y. (Xiaolei Yuan) embellished and checked the paper.

**Funding:** This research received no external funding.

**Acknowledgments:** Jianguo Zhou conceived the overall structure of the paper. Xuechao Yu wrote the paper. Xiaolei Yuan embellished and checked the paper.

**Conflicts of Interest:** The authors declare no conflict of interest.

## References

1. International Energy Agency (IEA). *World Energy Outlook 2007: China and India Insights*; International Energy Agency: Paris, France, 2007.
2. Yu, L.; Dai, W.; Tang, L. A novel decomposition ensemble model with extended extreme learning machine for crude oil price forecasting. *Eng. Appl. Artif. Intell.* **2015**, *47*, 110–121. [[CrossRef](#)]
3. Cheng, K.; Pan, G.; Smith, P.; Luo, T.; Li, L.; Zheng, J.; Zhang, X.; Han, X.; Yan, M. Carbon footprint of China's crop production—An estimation using agro-statistics data over 1993–2007. *Agric. Ecosyst. Environ.* **2011**, *142*, 231–237. [[CrossRef](#)]
4. Liao, Z.; Zhu, X.; Shi, J. Case study on initial allocation of Shanghai carbon emission trading based on Shapley value. *J. Clean. Prod.* **2015**, *103*, 338–344. [[CrossRef](#)]
5. Linda, P.; Marco, R.; Andrea, T.; Silvano, C. An Agent-based Stock-flow Consistent Model of the Sustainable Transition in the Energy Sector. *Ecol. Econ.* **2018**, *145*, 274–300. [[CrossRef](#)]
6. Zhang, Y.J.; Wei, Y.M. An overview of current research on EU ETS: Evidence from its operating mechanism and economic effect. *Appl. Energy* **2010**, *87*, 1804–1814. [[CrossRef](#)]
7. Guðbrandsdóttir, H.N.; Haraldsson, H.Ó. Predicting the price of EU ETS carbon credits. *Syst. Eng. Procedia* **2011**, *1*, 481–489. [[CrossRef](#)]
8. Lu, L.L.; Ma, X.; Wang, Y.X.; Yu, G.B. Lead price forecasting based on ARIMA model. *Adv. Mater. Res.* **2012**, *488*, 1582–1586. [[CrossRef](#)]
9. Chevallier, J. Carbon futures and macroeconomic risk factors: A view from the EU ETS. *Energy Econ.* **2009**, *31*, 614–625. [[CrossRef](#)]
10. Feng, Z.H.; Wei, Y.M.; Wang, K. Estimating risk for the carbon market via extreme value theory: An empirical analysis of the EU ETS. *Appl. Energy* **2012**, *99*, 97–108. [[CrossRef](#)]
11. Wang, Y.; Wu, C. Forecasting energy market volatility using GARCH models: Can multivariate models beat univariate models? *Energy Econ.* **2012**, *34*, 2167–2181. [[CrossRef](#)]
12. Zou, X.; Tian, L. Carbon price and international crude oil price fluctuations analysis based on ARMA\_GARCH model. *Int. J. Earth Sci. Eng.* **2014**, *7*, 2588–2593.
13. Faruk, D.Ö. A hybrid neural network and ARIMA model for water quality time series prediction. *Eng. Appl. Artif. Intell.* **2010**, *23*, 586–594. [[CrossRef](#)]
14. Koutroumanidis, T.; Ioannou, K.; Arabatzis, G. Predicting fuelwood prices in Greece with the use of ARIMA models, artificial neural networks and a hybrid ARIMA–ANN model. *Energy Policy* **2009**, *37*, 3627–3634. [[CrossRef](#)]
15. Zhao, L.; Cheng, L.; Wan, Y.; Zhang, H.; Zhang, Z.A. VAR-SVM model for crude oil price forecasting. *Int. J. Glob. Energy Issues* **2015**, *38*, 126–144. [[CrossRef](#)]
16. Zhu, B.; Wei, Y. Carbon price forecasting with a novel hybrid ARIMA and least squares support vector machines methodology. *Omega* **2013**, *41*, 517–524. [[CrossRef](#)]
17. Huang, N.E.; Shen, Z.; Long, S.R.; Wu, M.C.; Shih, H.H.; Zheng, Q.; Yen, N.C.; Tung, C.C.; Liu, H.H. The empirical mode decomposition and the Hilbert spectrum for nonlinear and non-stationary time series analysis. *Proc. R. Soc. Lond. A Math. Phys. Eng. Sci.* **1998**, *454*, 903–995. [[CrossRef](#)]
18. Huang, N.E.; Shen, Z.; Long, S.R. A new view of nonlinear water waves: The Hilbert Spectrum. *Annu. Rev. Fluid Mech.* **1999**, *31*, 417–457. [[CrossRef](#)]
19. Zhu, B. A novel multiscale ensemble carbon price prediction model integrating empirical mode decomposition, genetic algorithm and artificial neural network. *Energies* **2012**, *5*, 355–370. [[CrossRef](#)]
20. Zhu, B.; Chevallier, J. Forecasting carbon price using empirical mode decomposition and evolutionary least squares support vector regression. *Appl. Energy* **2017**, *191*, 521–530. [[CrossRef](#)]
21. Wu, Z.; Huang, N.E. Ensemble empirical mode decomposition: A noise-assisted data analysis method. *Adv. Adapt. Data Anal.* **2009**, *1*, 1–41. [[CrossRef](#)]
22. Yu, S.; Zhang, J.; Zheng, S.; Sun, H. Provincial carbon intensity abatement potential estimation in China: A PSO–GA-optimized multi-factor environmental learning curve method. *Energy Policy* **2015**, *77*, 46–55. [[CrossRef](#)]
23. Tang, L.; Dai, W.; Yu, L.; Wang, S. A novel CEEMD-based EELM ensemble learning paradigm for crude oil price forecasting. *Int. J. Inf. Technol. Decis. Mak.* **2015**, *14*, 141–169. [[CrossRef](#)]

24. Zheng, J.W.; Li, S.X.; Kun, Y.A. new hybrid model for forecasting crude oil price and the techniques in the model. *Adv. Mat. Res.* **2014**, *974*, 310–317. [[CrossRef](#)]
25. Li, T.; Zhou, M.; Guo, C.; Luo, M.; Wu, J.; Pan, F.; Tao, Q.; He, T. Forecasting crude oil price using EEMD and RVM with adaptive PSO-based kernels. *Energies* **2016**, *9*, 1014. [[CrossRef](#)]
26. Feng, Z.H.; Liu, C.F.; Wei, Y.M. How does carbon price change? Evidences from EU ETS. *Int. J. Glob. Energy Issues* **2010**, *35*, 132–144. [[CrossRef](#)]
27. Zhu, B.; Ye, S.; Wang, P.; He, K.; Zhang, T.; Wei, Y.M. A novel multiscale nonlinear ensemble leaning paradigm for carbon price forecasting. *Energy Econ.* **2018**, *70*, 143–157. [[CrossRef](#)]
28. Qi, S.; Zhao, X.; Tan, X. A study on the formation mechanism of Chinese carbon market price based on EEMD model. *Wuhan Univ. J.* **2015**, *4*, 56–65.
29. Li, W.; Lu, C. The research on setting a unified interval of carbon price benchmark in the national carbon trading market of China. *Appl. Energy* **2015**, *155*, 728–739. [[CrossRef](#)]
30. Zhao, X.G.; Jiang, G.W.; Nie, D.; Chen, H. How to improve the market efficiency of carbon trading: A perspective of China. *Renew. Sustain. Energy Rev.* **2016**, *59*, 1229–1245. [[CrossRef](#)]
31. Zhao, X.G.; Wu, L.; Li, A. Research on the efficiency of carbon trading market in China. *Renew. Sustain. Energy Rev.* **2017**, *79*, 1–8. [[CrossRef](#)]
32. Cortes, C.; Vapnik, V. Support-vector networks. *Mach. Learn.* **1995**, *20*, 273–297. [[CrossRef](#)]
33. Yan, J.; Tian, F.; Feng, J.; Jia, P.; He, Q.; Shen, Y. A PSO-SVM method for parameters and sensor array optimization in wound infection detection based on electronic nose. *J. Comput.* **2012**, *7*, 2663–2670. [[CrossRef](#)]
34. Rajasekaran, S.; Gayathri, S.; Lee, T.L. Support vector regression methodology for storm surge predictions. *Ocean Eng.* **2008**, *35*, 1578–1587. [[CrossRef](#)]
35. Kennedy, J.; Eberhart, R. Particle swarm optimization. In Proceedings of the IEEE International Conference on Neural Networks, Perth, WA, USA, 27 November–1 December 1995; pp. 1942–1948.
36. Han, F.; Yao, H.F.; Ling, Q.H. An improved evolutionary extreme learning machine based on particle swarm optimization. *Neurocomputing* **2013**, *116*, 87–93. [[CrossRef](#)]
37. Sun, W.; Wang, C.; Zhang, C. Factor analysis and forecasting of CO<sub>2</sub> emissions in Hebei, using extreme learning machine based on particle swarm optimization. *J. Clean. Prod.* **2017**, *162*, 1095–1101. [[CrossRef](#)]
38. Huang, G.B.; Zhu, Q.Y.; Siew, C.K. Extreme learning machine: Theory and applications. *Neurocomputing* **2006**, *70*, 489–501. [[CrossRef](#)]
39. Pan, H.X.; Cheng, G.J.; Cai, L. Comparison of the extreme learning machine with the support vector machine for reservoir permeability prediction. *Comput. Eng. Sci.* **2010**, *31*, 131–134. [[CrossRef](#)]
40. Zhang, X.; Lai, K.K.; Wang, S.Y. A new approach for crude oil price analysis based on Empirical Mode Decomposition. *Energy Econ.* **2008**, *30*, 905–918. [[CrossRef](#)]

